Meteorologische Zeitschrift, Vol. **23**, No. 4, 369–385 (published online August 27, 2014)

Modeling artifacts in the simulation of the sedimentation of raindrops with a Quadrature Method of Moments

Gary Jasor[1]*, Ulrike Wacker[2], Klaus Dieter Beheng[3] and Wolfgang Polifke[1]

[1]Technische Universität München, Garching, Germany
[2]Alfred-Wegener-Institut Helmholtz Zentrum für Polar- und Meeresforschung, Bremerhaven, Germany
[3]Institute for Meteorology and Climate Research, Karlsruhe Institute of Technology, Karlsruhe, Germany

(Manuscript received December 17, 2013; in revised form April 8, 2014; accepted June 9, 2014)

Abstract

The Quadrature Method of Moments (QMoM) is applied to a one-dimensional test case for sedimentation of raindrops. Comparison of the results with a reference spectral method exhibits discrepancies ("step patterns") that must be considered as modeling artifacts. As the QMoM has been demonstrated to be effective and accurate in various contexts, the origin of these artifacts is investigated and found to be related to the transport of the quadrature abscissas. Further test cases are considered to examine the influence of different initial conditions on the development of the modeling artifacts. The study shows that these artifacts are inherent to the application of QMoM in pure sedimentation context.

Keywords: Quadrature Method of Moments, Sedimentation, Raindrops, Modelling artifacts

1 Introduction

The spatio-temporal development of particulate matter in terms of size distributions is generally described by a balance equation comprising all relevant processes and mechanisms as transport, phase changes as well as nucleation, mutual collisions, aggregation, breakup and more. This equation, having its roots in the well-known Boltzmann transport theorem (Pitaevskii and Lifshitz, 1981), is named in technical applications the population balance equation (PBE) (Ramkrishna, 2000) and is known in meteorological issues as spectral balance equation (SBE) (Pruppacher and Klett, 1997). This equation, which in the following will be referred to as PBE and SBE synonymously, is strictly non-linear and contains – if collisional interactions (in the widest sense) are considered – integral terms with mostly complex integrands, as well as integral limits, such that its solution is in general only possible numerically.

The most detailed method to numerically solve PBE or SBE, respectively, is to discretize the size range of particles and consequently its corresponding particle size distribution (PSD) function in large a number of bins, for which the rate equations are integrated in space and time. But note that in cloud microphysical applications the size range of particles (cloud droplets, raindrops, ice crystals, graupel, hail) span several orders of magnitudes, such that also the numerical solution can be very complex and costly. Nevertheless, several attempts were successful to numerically compute the solution of SBE reliably in great detail and with great accuracy and have been applied in so-called cloud models, see e.g. Berry and Reinhardt (1974); Khain and Sednev (1996). The drawback of this method is that – just because of the high costs – its application in, e.g., numerical weather prediction (NWP) models for simulating the evolution of clouds and precipitation is out of scope.

Therefore meteorologists have developed methods to overcome this drawback in that not the particle size distributions have been predicted, but only some moments of them (see below). And at this point the idea of the priority program METSTRÖM (meteorology and fluid mechanics) sponsored by the German Science Foundation (Deutsche Forschungsgemeinschaft, DFG) comes into play, namely to bring together scientists from several disciplines dealing with same problems. Problems of the kind described above are also faced by hydrodynamicists and engineers as, e.g., polydisperse flows in multi-phase reactors, spray vaporization, combustion processes or solid particle sedimentation. The common problem that is tackled in this paper by hydrodynamicists and meteorologists in a joint effort is the numerical calculation of a single process captured by the PBE: pure gravitational sedimentation of differently sized cloud droplets and raindrops resulting eventually in a rain event at ground.

It should be anticipated that also in calculating this simple mechanism a number of problems arises. But before we start with the investigation the different methods applied by hydrodynamicists and meteorologists are briefly presented. Both have developed and applied what is called the *Method of Moments* (MoM).

*Corresponding author: Gary Jasor, Lehrstuhl für Thermodynamik, Technische Universität München, Boltzmannstraße 15, 85747 Garching, Germany, e-mail: jasor@td.mw.tum.de

DOI 10.1127/0941-2948/2014/0590
Gebrüder Borntraeger Science Publishers, Stuttgart, www.borntraeger-cramer.com

1. For many years meteorologists have circumvented the problem of the expensive detailed solution of SBE by deriving rate equations for certain moments of the PSD as for example see Kessler (1969); Milbrandt and Yau (2005); Seifert and Beheng (2006). These moments, whose definitions are given in section 2, are the number density, the mass density (mostly named liquid water content) and, if a third moment is desirable or necessary, the radar reflectivity. The choice of these moments is guided by the consideration of the possibility to compare their calculated values with observations/measurements. A set of prognostic equations for these moments in integral form can in general be formulated. Their solution, however, usually cannot be done without several simplifications and assumptions, which render this procedure problematic. Indeed, a severe drawback is the closure problem, as integration of SBE sometimes requires moments, whose degree is different from those for which equations are available. This problem can be solved by the assumption of specific master functions for the PSD; hence we also speak of Presumed function Method of Moments or PMoM.

   The application of such PMoMs in NWP models reduces the computational costs largely such that these equations are already used in test versions of operational weather forecast systems (Seifert et al., 2012).

2. Simultaneously hydrodynamicists have developed other types of moment methods. The number of moments to be considered is variable, typically at most six moments are considered. The solution method Quadrature Method of Moments or QMoM (McGraw, 1997) is based on the application of specific numerical quadrature formulae as, e.g. Gaussian, with which the moments' integrals are approximated. It is interesting to note that while this method has been successfully applied to various fields (e.g. Acher et al., 2013), the first idea on QMoM stemmed from a problem of aerosol dynamics, a special part of cloud microphysics. A severe challenge of QMoM is - besides also suffering from a closure problem – that some conditions (see below in subsection 2.2) can occasionally lead to the unrealizability of the set of moments, i.e. for a set of moments there exists no PSD (cf. Hankel-Hadamard positivity, Handy et al., 1988). A further development of QMoM is the Direct Quadrature Method of Moments (DQMoM) by Marchisio and Fox (2005), which circumvents the unrealizability problem. The attractive feature of both methods, also for meteorological applications, is ostensibly their low computational demand with simultaneous accuracy, which is checked here. Further details on the MoMs are given in section 2.2 and 2.3 of the main text.

The topic of this study is to assess the ability of two moments methods to accurately describe the pure sedimentation of cloud droplet and raindrops in a one-dimensional geometry, i.e. with a so-called rainshaft model. The motivation comes from results of a companion paper by Ziemer et al. (2014), wherein the same setup has been chosen as in this study and step patterns in the numerical results of the vertical profiles of moments of cloud parameters have been observed. This feature can be traced back to the application of various MoMs methods, as the usage of the detailed calculation by means of a numerical solution of the spectral balance kinetic equation (SBE) does not show this artifact.

The paper is organized as follows. In section 2 the basic equations, especially the sedimentation equation in one-dimension and the quadrature methods are presented. First applications are shown in section 3 comparing the results of the moments methods with that of considering the detailed solution of SBE for the one-dimensional geometry, i.e. the rainshaft. These results are supplemented by an in-depth discussion of artifacts appearing. In order to explain the artifacts, in section 4 different influencing factors are investigated and thoroughly discussed: the influences of the initial shape of the PSD, of the non-homogeneous abscissas and of the spatial discontinuities. Section 5 concludes this study.

2 The model and the Quadrature Methods of Moments

2.1 Basic equations

In this article, we will concentrate on the single process of sedimentation of drops and use the same set up as in the companion paper by Ziemer et al. (2014). The PBE for the PSD f_D reduces for the spatially one-dimensional pure sedimentation problem to

$$\frac{\partial f_D(D,z,t)}{\partial t} - \frac{\partial V_T(D,z,t) f_D(D,z,t)}{\partial z} = 0, \qquad (2.1)$$

where D is the drop diameter, t is the time, z is the height, and V_T is the downward directed fall velocity; we use for V_T the model of a drop falling in quescient air under the balance of forces. V_T increases with drop size, and a widely used analytic fit $V_T(D)$ is (see Kessler, 1969):

$$V_T(D) = \alpha \left(\frac{D}{D_v} \right)^{\beta}, \qquad (2.2)$$

where α, D_v and β are constants ($\alpha = 13\,\mathrm{ms}^{-1}$, $\beta = 0.5$, $D_v = 10^{-2}\,\mathrm{m}$). The size-dependency of the particle velocity is known as *poly-celerity* (Dems et al., 2012).

Defining the moment of order k as

$$M^{(k)}(z,t) = \int_{D=0}^{\infty} D^k f_D(D,z,t) dD, \qquad (2.3)$$

multiplication of the PBE by D^k ($k \geq 0$), and integration over the diameter range, yields the Moment Transport

Equation (MTE):

$$\frac{\partial M^{(k)}(z,t)}{\partial t} - \frac{\partial U^{(k)}(z,t) M^{(k)}(z,t)}{\partial z} = 0. \tag{2.4}$$

Here $U^{(k)}$ is the velocity with which the k-th moment is transported. The following equation gives the definition of $U^{(k)}$ and its dependency on the moments, when using equation (2.2):

$$\begin{aligned} U^{(k)}(z,t) &= \frac{1}{M^{(k)}(z,t)} \int_0^{+\infty} V_T(D) D^k f_D(D,z,t) dD \\ &= \frac{\alpha}{{D_v}^{\beta}} \frac{M^{(k+\beta)}(z,t)}{M^{(k)}(z,t)}. \end{aligned} \tag{2.5}$$

Note that, for the sake of brevity, we will not explicitly indicate the height and time dependency in the following.

Equation (2.5) makes explicit a so-called closure problem, which does not arise in the spectral formulation. This closure problem originates from the poly-celerity (size-dependency). Indeed, all moment velocities $U^{(k)}$ would be equal to V_T, if the latter were independent of the diameter. On the other hand, if velocity depends on the diameter (as it is the case here), that is $V_T = V_T(D)$, each moment is transported with a different velocity. Now, when only moments are considered, we distinguish between those moments $M^{(k)}$, which are transported according to equation (2.4) and are called "prognostic", and any other moments (which are called "diagnostic"), such as e.g., $M^{(k+\beta)}$. Information is required about this moment to evaluate $U^{(k)}$ and thus to forecast $M^{(k)}$ from equation (2.4). Several approaches exist as closure assumption. As a first example we mention the widely used Presumed function Method of Moments (PMoM), which basically consists in assuming a given analytical form for the PSD, which allows for calculating analytically any unknown moments (Clark, 1974; Beheng, 1994; Seifert and Beheng, 2006; Ziemer et al., 2014; Dems et al., 2012). Further examples, and these will be used here, are the Quadrature Method of Moments (QMoM) and its derived version, the Direct Quadrature Method of Moments (DQMoM), which achieve closure thanks to the Gaussian Quadrature. Note that, in case equation (2.1) has source terms (to model population dynamics as breakup or coalescence for example), closure has to be achieved also for resulting source terms in the MTE.

2.2 QMoM

The Quadrature Method of Moments (QMoM), as introduced by McGraw (1997), is based on the Gaussian quadrature. The N_q-points Gaussian quadrature consists in an approximation of the integral of the product of a distribution function $f(x)$ with internal coordinate x and an arbitrary function $\varphi(x)$ (provided this integral is well defined) by a weighted sum of evaluations of this φ-function at given values:

$$\int_0^{\infty} \varphi(x) f(x) dx \simeq \sum_{i=1}^{N_q} \varphi(\xi_i) w_i, \tag{2.6}$$

The approximation is exact for polynomial functions of degree $2N_q - 1$ or less. The so-called weights are denoted by w_i. The so-called abscissas ξ_i are the values of x at which the function is evaluated and are denoted so that $\xi_1 < \xi_2 < \xi_3 < \ldots$.

Applying the Gaussian quadrature to $M^{(k)}$, we obtain

$$M^{(k)} = \sum_{i=1}^{N_q} {\xi_i}^k w_i \tag{2.7}$$

and can thus solve the closure problem resulting from poly-celerity, as we are able to estimate $M^{(k+\beta)}$ as:

$$M^{(k+\beta)} = \sum_{i=1}^{N_q} {\xi_i}^{k+\beta} w_i. \tag{2.8}$$

Note that for the integrated form of the PBE, any term involving an integral over the diameter range and involving the PSD, can be estimated the same way (in particular potential source terms).

QMoM can be seen as the use of N_q δ-functions (Dirac) to represent the PSD with a coarsely discretized internal coordinate D, whose nodes would correspond to the abscissas. Despite the coarse resolution, QMoM can achieve high accuracy, because it places the abscissas and calculates the respective weights in an optimal manner in order to fit the moment series. See for illustration Fig. 1, which shows in the left part several PSDs $f_D(D)$ and in the right part a selected PSD along with the abscissas ξ_i and weights w_i for $N_q = 3$.

The main issue is then to be able to determine the corresponding abscissas and weights. According to Gordon (1968), this can be done by using the so-called Product-Difference Algorithm (PDA). Out of the first $2N_q$ moments ($M^{(0)}$ to $M^{(2N_q-1)}$), one can determine N_q abscissas and N_q weights by constructing a symmetric matrix and solving an eigenvalue problem, where the abscissas are the eigenvalues of this matrix and the weights proportional to the first component of the corresponding eigenvectors. Some alternatives to the PDA have been considered to determine the abscissas and weights (for example in John and Thein, 2012), but we will not discuss them here.

QMoM has the advantage of dealing with a system of $2N_q$ equations, whereas a spectral formulation often involves more than hundred classes in order to guarantee a smooth resolution of the PSD and independence of discretization. It has been demonstrated (Marchisio et al., 2003) that choosing N_q to be equal to 3 provides good results and a good tradeoff to computational costs, which means that we will need to transport the first six moments of the PSD. The computational costs are

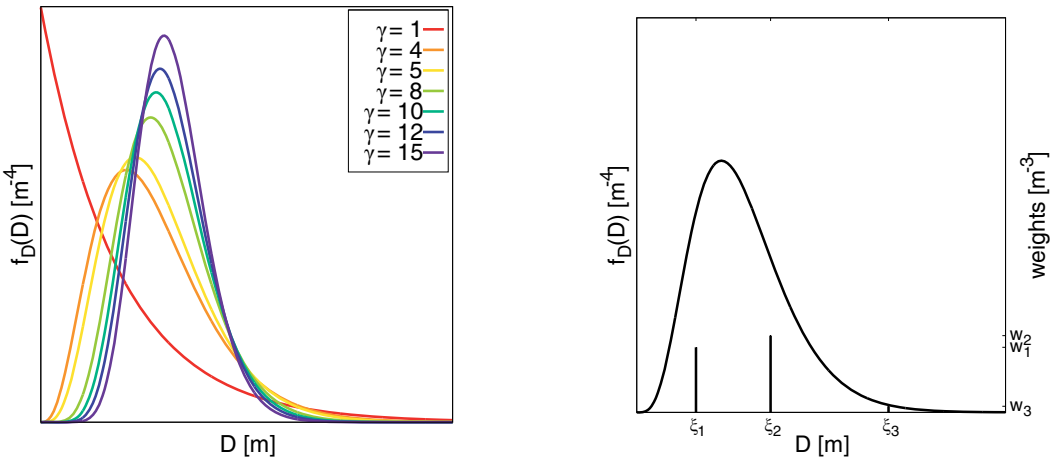

Figure 1: Illustration of drop size distributions (PSD) and the concept of QMOM. Left: Influence of the variation of the shape parameter γ of a Γ-Distribution from equation (3.1) for fixed number density N and liquid water content L. Right: Relationship between Γ-Distribution with $\gamma = 5$ and the abscissas ξ_i weights w_i, that are the heights of the bars, according to QMOM.

thereby drastically reduced. Moreover, no assumption is necessary for the analytical form of the PSD. Notwithstanding those advantages, an important feature (which is common to other MoMs) is that the transport of the moments possibly leads to the well known *problem of moments* (also "unrealizability of moments"), when no PSD can be found that matches a given set of moments (Curto and Fialkow, 1991; Shohat and Tamarkin, 1943). This issue can make it impossible to carry on the simulation (cf. Wright Jr, 2007). This problem is even of greater importance if one considers that the PDA is prone to be sensitive to numerical discrepancies (John and Thein, 2012). Some criteria exist in order to assess the realizability of a set of moments (especially the so-called Hankel-Hadamard Determinants, Handy et al., 1988). Fortunately, the criterion of realizability is always fulfilled in our simulations. The diligent reader should note that in a general context, unrealizability events can be enhanced by a high number of prognostic moments (more degrees of freedom for the set of moments), by effects on the population dynamics such as coalescence or breakup, or by different transport velocities for the moments due to poly-celerity (size-dependency).

In the present case of pure non-linear advection equations, the resolution is quite straightforward (e.g. with a first order upwind scheme). Hence, our test cases should not a priori fall in the range of problematic configurations.

2.3 DQMoM

In order to circumvent the underlying limits of the QMoM (in particular unrealizability of the set of moments and the use of the PDA) an alternative approach has been proposed by Marchisio and Fox (2005): the Direct Quadrature Method of Moments (DQMoM). While for the QMoM the abscissas and weights are obtained from the transported moments, in this approach, the basic idea is to transport directly the abscissas and the weights (and thus eventually reconstruct the moments from them). As the derivation of the transport equations for the abscissas and the weights is based on the MTE, the two methods are essentially equivalent. The transport equations for abscissas and weights are given by:

$$\frac{\partial w_i}{\partial t} - \frac{\partial V_T(\xi_i) w_i}{\partial z} = 0 \tag{2.9a}$$

$$\frac{\partial \zeta_i}{\partial t} - \frac{\partial V_T(\xi_i) \zeta_i}{\partial z} = 0 \tag{2.9b}$$

with $\zeta_i = \xi_i w_i$, $i \in \{1,2,3\}$ and $V_T(\xi_i)$ given by equation (2.2) as:

$$V_T(\xi_i) = \alpha \left(\frac{\xi_i}{D_v} \right)^{\beta}. \tag{2.10}$$

Each weight w_i and weighted abscissa ζ_i is therefore transported with a characteristic velocity $V_T(\xi_i)$, which is the terminal fall velocity of a particle of diameter ξ_i. Further details on the derivation of transport equations for the weights and the abscissas (which directly stems from Marchisio and Fox, 2005), are given in appendix A.

The same closure approach as in QMoM (Gaussian quadrature) is then applied to estimate the diagnosed values.

Compared to QMoM, we obtain a set of equations of similar complexity for the pure sedimentation context. Nevertheless in a more general scope, the DQMoM involves additional source terms, which have to be determined through the resolution of a linear system. This linear system can be seen as the counterpart of the PDA in the QMoM approach and might not be straightforward to derive and solve in a general scope. These constraints should guide one in the choice of the preferred approach.

3 Reference study case: one dimensional pure sedimentation of water drops

3.1 Presentation of the reference study case

In this section, we present the reference test case, which makes explicit the main issue of this article, that is the appearance of modeling artifacts in the simulation of sedimentation. The model consists in a one dimensional configuration with an initial homogeneous cloud confined between two heights (namely 8250 m and 9750 m). Only sedimentation is taken as relevant for the evolution of drop distributions. The geometric configuration is similar to the so-called rainshaft model (Seifert and Beheng, 2001), but without coagulation.

We consider the space domain to be 10000 m high (discretized with $N_p = 1601$ points and intervals $\Delta z = 6.25$ m apart); the large domain is chosen not because of cloud physical relevance, but by reason of illustration of the evolution of the relevant properties in time. The numerical solution of the transport equations is done by using an explicit first-order upwind scheme (Patankar, 1980), with a time step $\Delta t = 0.2$ s (meaning CFL numbers less than 0.3 for all methods). The PSD is initialized everywhere with a Γ-distribution such that:

$$f_D(D,z,0) = n_0 \frac{D^{\gamma-1} e^{-D/\lambda}}{\Gamma(\gamma)\lambda^{\gamma}} \tag{3.1}$$

where n_0, γ and λ are the given parameters of the Γ-distribution ($n_0 = 1.2 \times 10^4\,\mathrm{m}^{-3}$, $\gamma = 1$ and $\lambda = 2.367 \times 10^{-4}$ m). Those values depict a liquid water content L of $5 \times 10^{-4}\,\mathrm{kgm}^{-3}$, a total number density $N = n_0$ of $1.2 \times 10^4\,\mathrm{m}^{-3}$ and are the values considered in one of the test cases presented in the companion paper by Ziemer et al. (2014). Further information on the setup can be found in Mukhopadhyay et al. (2012); Ziemer and Wacker (2012); Ziemer et al. (2014).

One important issue is the initialization of the population outside the cloud. Indeed, this region is void of particles, but the moments (and therefore the PSD) cannot be taken exactly equal to zero to prevent MTE of the form "0 = 0" in the solution algorithm. Since there is no physical guideline for the choice of those values outside the cloud, we initialize the fields in a straightforward way and assume the same distribution as inside the cloud, but reducing the parameter n_0 (actually $M^{(0)}$) in equation (3.1) by multiplication with a scale factor (10^{-8}), so that it becomes negligible. This choice has, however, considerable effects on the simulation, as will be discussed later. Finally, as upper boundary condition we adopt the Dirichlet conditions and fix here the initial values outside the cloud, that is no drops enters the domain. The lower boundary is open for the outflux of condensate.

For the spectral reference model, the diameter range is discretized into 500 classes of non-equal lengths $\Delta D_k = D_{k1/2} - D_{k-1/2}$, the spectral number density within an interval ΔD_k around D_k is given by

$$ND(D_k) = \int_{D \in \Delta D_k} f_D(D)dD \simeq f_D(D_k)\Delta D_k. \tag{3.2}$$

The distribution $ND(D_k)$ or, skipping the arbitrary index k, $ND(D)$ is proportional to the respective diameter interval. $ND(D)$ and $f_D(D)$ provide different spectral measures for the same drop ensemble.

The evolution of our model system will be discussed in terms of the three moments $M^{(0)}$, $M^{(3)}$ and $M^{(6)}$. They are of particular relevance in cloud physics, as they are related to the total number density ($N = M^{(0)}$), the liquid water content ($L = M^{(3)}\rho_w\pi/6$ with ρ_w: bulk density of liquid water) and the radar reflectivity ($Z = M^{(6)}$). In QMoM $M^{(0)}$, $M^{(3)}$ are prognostic moments, whereas $M^{(6)}$ is the first diagnosed one. Figure 2 shows the temporal evolution of the vertical profiles of these three moments, as well as the corresponding abscissas ξ_i and weights w_i. The results for the QMoM and the DQMoM (which are almost identical) are plotted in comparison with the results of a spectral formulation. The quantities of interest are depicted on the x-axis and the height on the y-axis. For the spectral results, the abscissas ξ_i and the weights w_i are reconstructed from the moments with the PDA.

In Fig. 3, we present the temporal evolution of the spectral number density $ND(D)$ at different heights, namely 5000, 7000 and 9000 m, which were chosen such that the last one is within the cloud layer at initial conditions and the others below it. We compare these results to the abscissas ξ_i and weights w_i at the same heights. In the Figure, the diameter is depicted on the x-axis, while the left and right y-axes represent ND and the corresponding weights w_i, respectively. Note that the abscissas ξ_i for the spectral method are indicated on the bottom x-axis and those for QMoM on the upper one.

3.2 Discussions

The general features of the vertical profiles of the moments are correctly reproduced by the QMoM (first three columns in Fig. 2). Indeed, the different moments descend with their moment velocities ($U^{(k)}$, cf. eq. (2.5)), the higher the order of the moment, the faster it progresses downwards. This is due to the fact that the higher the order of the moment, the more it is determined by the biggest drops, which fall faster than the smaller ones.

All moment-profiles in Fig. 2 show "step"-patterns already after 400 s. The pattern becomes more pronounced with time and eventually leads to the formation of a second maximum, as can be seen for $M^{(3)}$ already after 800 s at around 5000 m. The occurrence of such steps was also noted by Ziemer et al. (2014), see their Fig. 1 for $N(t,z)$ and $L(t,z)$, and as an outcome the multi-peaked surface precipitation in their Fig. 2. These features neither have a counterpart in the moment profiles from the spectral model, nor can they be

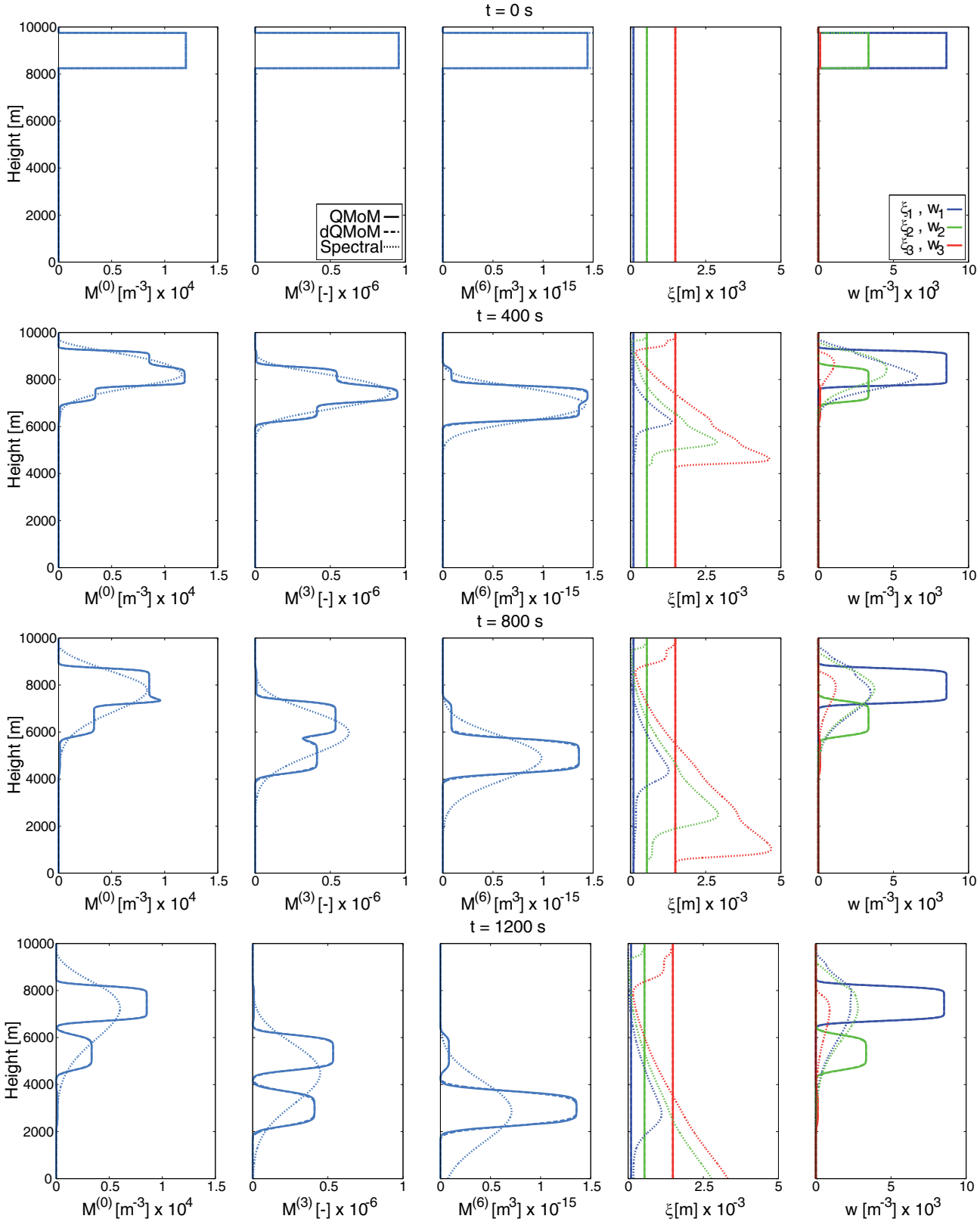

Figure 2: Reference study case: Time evolution of the vertical profiles of the moments $M^{(0)}$, $M^{(3)}$, $M^{(6)}$ ($M^{(0)} = N$ is total number density, $M^{(3)} = L(\pi/6\rho_w)^{-1}$ is proportional to liquid water content, $M^{(6)} = Z$ is radar reflectivity), abscissas ξ_i and weights w_i. The quantities are given for model times $t = 0$, 400, 800, 1200 s. Solid line: QMoM. Dashed line: DQMoM (mainly overlapping QMoM). Dotted line: spectral method (reference). First, second and third couple of abscissa and weight are plotted in blue, green and red, respectively.

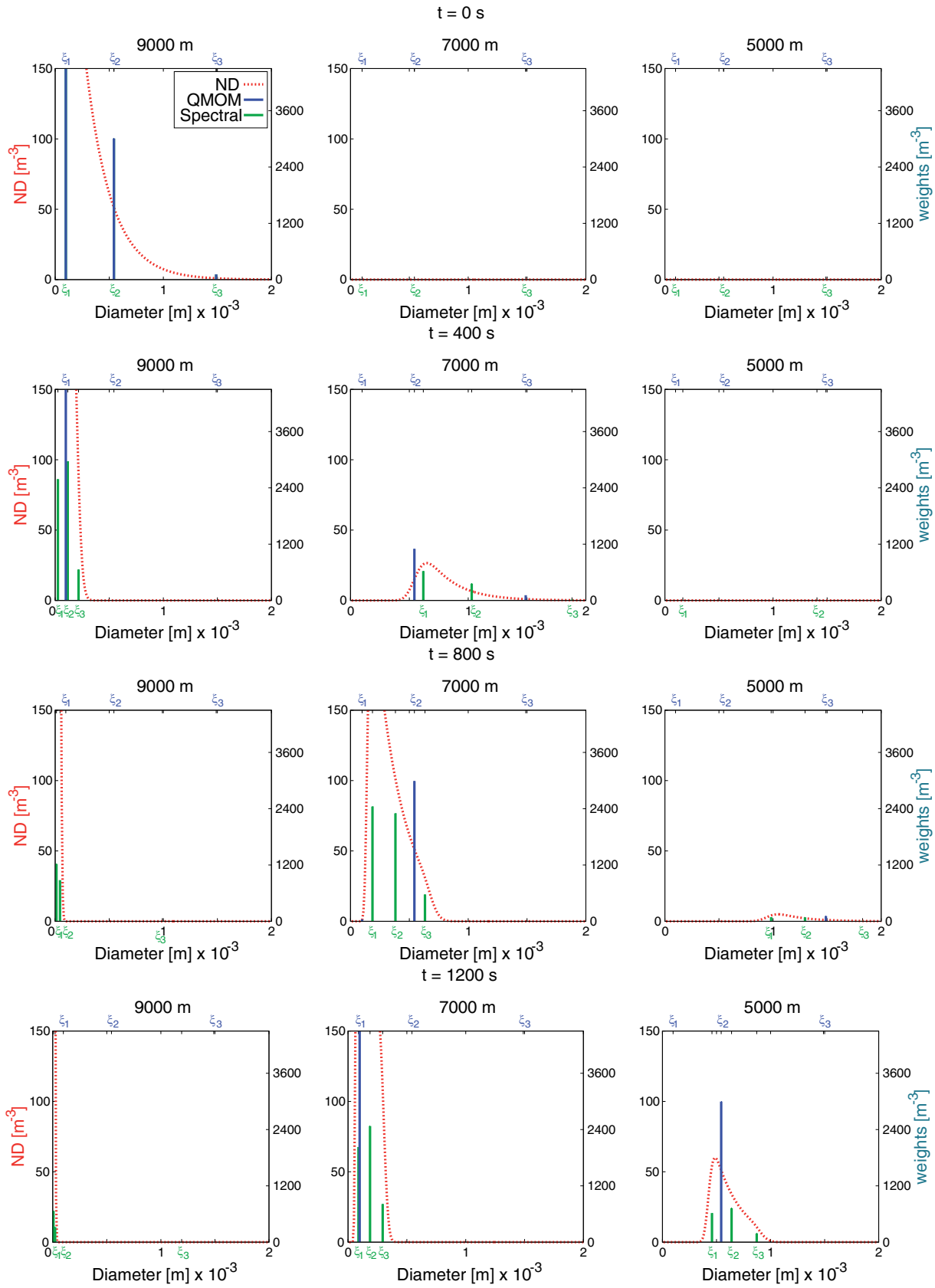

Figure 3: Reference study case: time evolution of spectral number density $ND(D)$ from spectral model (red dotted line, left ordinate) at 9000 m, 7000 m and 5000 m and corresponding abscissas ξ_i and weights w_i (right ordinate) for spectral model (green) and QMoM (blue). The abscissas ξ_i for the spectral model (green) are specified on the bottom diameter axis, and for QMoM (blue) on the top axis. For clarity, the ordinate is capped in some subfigures.

explained physically. Hence they have to been considered as modeling artifacts of the QMoMs. The sole analysis of the profiles of the moments is not sufficient to understand the occurrence of these artifacts.

A closer look is therefore taken at the profiles of the abscissas and the weights (see two last columns in Fig. 2). It can be seen that the initial conditions imply a vertically homogeneous profile for the abscissas ξ_i, that is to say "constant" over the height (as opposed to constant in time or stationary). Indeed, the positions of the abscissas ξ_i depend on the shape of the initial PSD and since the latter is assumed to be the same (apart from the scaling factor) over the height at initial conditions, the abscissas should be homogeneous initially. However, the QMoM results show that the profiles of the abscissas are stationary, while they change in both space and time for the spectral formulation. Specifically, the spectral model abscissas ξ_i increase with time at the bottom of the cloud, as the population is more and more composed of the largest drops for this region. The opposite effect occurs at the upper boundary of the cloud, where only the smallest drops are present. We hence see a major difference in the way the spectral and the QMoM model depict the evolution of the abscissas, notably at the cloud boundaries.

This significant difference gives a clue to the origin of the steps in the profiles mentioned above. An explanation for this behavior may be developed by inspection of the transport equations of the weights and abscissas in the DQMoM context (equations (2.9)). If we consider the abscissas ξ_i as homogeneous (which holds in this reference case) and inject this in (2.9b), it can be written:

$$\begin{aligned} 0 &= \frac{\partial \zeta_i}{\partial t} - \frac{\partial V_T(\xi_i)\zeta_i}{\partial z} \\ &= w_i \frac{\partial \xi_i}{\partial t} + \xi_i \underbrace{\left(\frac{\partial w_i}{\partial t} - \frac{\partial V_T(\xi_i) w_i}{\partial z} \right)}_{=0 \text{ cf. (2.9a)}} - V_T(\xi_i) w_i \underbrace{\frac{\partial \xi_i}{\partial z}}_{\Rightarrow 0}. \end{aligned} \tag{3.3}$$

If ξ_i is independent of z in the initial state, it follows that $\partial \xi_i / \partial t = 0$, and ξ_i will be independent of height forever. In this case, we deduce that the shape of the profiles of the moments over the height is only determined by the shape of the vertical profiles of the weights (as the moments are the sum of the weights multiplied by ${\xi_i}^k$). Most important, each weight w_i is transported with its own constant velocity $V_T(\xi_i)$, whereby $V_T(\xi_1) < V_T(\xi_2) < V_T(\xi_3)$, such that the ranges of noteworthy weight-values separate. This is nicely seen in Fig. 2 for the first and second weights around 7000 m after 800 s. This segregation of the weights results into the "step" structure for the moments. Note that the effect appears at different heights depending on the order of the moment, as the weighting coefficient is different in the sum of the ${\xi_i}^k w_i$.

Knowing the velocity $V_T(\xi_i)$ with which each weight is transported, one is able to determine the time after which step patterns are expected to be visible. In our case, if H_T is the thickness of the cloud at initial conditions (here 1500 m), the instant t_{ij} when the two weights w_i and w_j ($1 \leq i < j \leq 3$) are split apart entirely can be expressed as:

$$t_{ij} = \frac{H_T {D_v}^\beta}{\alpha({\xi_j}^\beta - {\xi_i}^\beta)}. \tag{3.4}$$

Considering that the initial values for the abscissas of the reference test case are $\xi_1 = 9.8417 \times 10^{-5}$ m, $\xi_2 = 5.4307 \times 10^{-4}$ m and $\xi_3 = 1.4889 \times 10^{-3}$ m, we find $t_{12} \simeq 862$ s, $t_{13} \simeq 402$ s and $t_{23} \simeq 755$ s. This situation is seen in Fig. 2. After 800 s, the weights 1 and 2 are indeed about to split, and after 1200 s they have fully separated. Although weight 3 is very low, one sees that the weights w_1 and w_3 have nearly (fully) separated after 400 s (800 s), and that after 800 s w_2 and w_3 have just completely separated; the latter case results in a local minimum for the third moment. Moreover, a lower value for t_{13} than for the two other split times is in line with the fact that the two corresponding abscissas ξ_1 and ξ_3 are furthest from each other and therefore maximize the denominator in equation (3.4).

In Mukhopadhyay et al. (2012), the profiles of the moments do not exhibit strong step patterns, as it is the case in the present article. We offer the following explanations for the absence of clearly visible artifacts: firstly, the numerical scheme used for the discretization of the transport equation in the former work (i.e. Lax-Friedrich scheme) is known to be more diffusive than the upwind scheme used in the present work, secondly the space grid used by Mukhopadhyay et al. (2012) is coarser than the one presented here and finally, the cloud top being placed only at a height of 4000 m, we argue in line with (3.4) that the profiles of the weights overlap during their shorter simulation time as compared to our case, resulting in less visible artifacts. Note that in the present work, the space intervals were chosen such that the grid is fine enough to depict correctly the sharp discontinuities in the vertical profiles of the moments (or the weights). The coarser the grid is taken the more "rounded" these profiles become.

We now have a closer look at the evolution of the abscissas as predicted by the spectral model, given in Fig. 3. For the height level of 9000 m, that is within the initial cloud layer, the abscissas evolve towards the smaller diameters with time, as the population is dominated by the smallest drops, since the larger ones have settled rapidly. For the height levels 7000 m and 5000 m, that is below the initial cloud layer, the abscissas first move from their initial positions towards the bigger diameters, as the biggest drops reach the corresponding height, then migrate towards smaller diameters when the biggest drops have passed and the smaller ones arrive. These features cannot be depicted by the QMoM in this case with ξ_i constant both in space and time, since it is limited to changing the values of the weights w_i.

Table 1: Influence of initial shape of the PSD: split times t_{ij} according variation of the shape parameter γ of a Γ-distribution. Model conditions as used in Subsection 4.1 with $N = 3 \times 10^3\,\mathrm{m}^{-3}$ and $L = 5 \times 10^{-4}\,\mathrm{kgm}^{-3}$.

γ [-]	ξ_1 [m]	ξ_2 [m]	ξ_3 [m]	t_{12} [s]	t_{13} [s]	t_{23} [s]
1	1.5623×10^{-4}	8.6208×10^{-4}	2.3635×10^{-3}	684	319	599
4	2.9640×10^{-4}	7.3581×10^{-4}	1.4595×10^{-3}	1164	550	1042
5	3.2124×10^{-4}	7.2578×10^{-4}	1.3653×10^{-3}	1280	606	1153
8	3.7273×10^{-4}	7.1022×10^{-4}	1.2024×10^{-3}	1571	751	1438
10	3.9625×10^{-4}	7.0489×10^{-4}	1.1396×10^{-3}	1737	833	1601
12	4.1483×10^{-4}	7.0129×10^{-4}	1.0942×10^{-3}	1887	908	1749
15	4.3664×10^{-4}	6.9766×10^{-4}	1.0449×10^{-3}	2091	1009	1952

To sum up the findings from the reference case, we see that the initially homogeneous profiles of the abscissas result in a steady state ξ_i-profile in the QMOM-model. Therefore we should anticipate obvious deviations in the evolution of the moments, as indeed have been seen in Fig. 2. This raises the issue to modify the initial setup with regard to the selected shape of the initial PSD, non homogeneous abscissas and the vertical transition at the cloud boundaries. In the next section, we present three test cases designed to characterize the impact of each of these features on the modeling artifacts identified in the QMoM results. Each of these cases is independently designed in order to show the corresponding feature most clearly.

4 Test cases: impact of the initial conditions on the modeling artifacts

4.1 Influence of the initial shape of the PSD

In the first test case the initial shape of the PSD is changed. Again a Γ-function is assumed, but now the shape parameter γ in equation (3.1), which was set $\gamma = 1$ in Section 3, varies between 1 and 15. With increasing γ, the PSD describes a narrower spectrum (Fig. 1); likewise, the abscissas will be located at different points. The total number density N (i.e. $M^{(0)}$) is now set to $3 \times 10^3\,\mathrm{m}^{-3}$ and the liquid water content L (and thus $M^{(3)}$) is set as before. Without limiting the relevance of the study, this choice results in comparable time scales between the results for the different values of γ considered and allows for a faster development of the relevant effects (the results are therefore considered only up to 800 s). With the three pieces of information N, L and γ, the three parameters are calculated. The values of the abscissas and the weights for $\gamma = 5$ are sketched in the right part of Fig. 1. The temporal evolution of the profiles of $M^{(0)}$, $M^{(3)}$ and $M^{(6)}$ for the QMoM are presented in Fig. 4, and the derived split times t_{ij} (cf. eq. (3.4)) are listed in Table 1.

Figure 4 reveals that the shape of the PSD at initial conditions has a significant impact on the evolution of the vertical profiles of the moments. With increasing γ, (i) shift of the various moments becomes more alike and the signals stay more compactly, and (ii) the steps and the segregation effect become weaker. If γ is large (e.g., 12 or 15) the system is less prone to generate noticeable artifacts than in case of smaller values at the same time. The case $\gamma = 1$, corresponding to an exponential distribution, appears to be the most critical. Building on the analysis in the previous section, this behavior may be explained as follows: with increasing γ (cf. Fig. 1) the spectrum becomes narrower, hence the corresponding abscissas ξ_i are closer to each other and the differences in the transport velocities for the weights (given by eq. (2.10)) are smaller. This must lead to weaker segregation effects than in the reference case with $\gamma = 1$.

This behavior is confirmed by the analysis of the split times t_{ij} (Table 1). For all the γ considered here, the largest split time (corresponding therefore to the time where all weights are separated) is t_{12} and this value increases as the shape parameter γ becomes larger, such that segregation occurs first for $\gamma = 1$ at $t_{13} = 319\,\mathrm{s}$, which is only about one third of the value for $\gamma = 15$. In fact, we see in Fig. 4 in the latter case, a compact signal of moments without any steps.

This case study shows that a broad PSD is prone to the formation of steps and segregation effects, while for a narrow PSD the occurrence of the artifacts is retarded and for a monodisperse spectrum prevented. This result is in line with the arguments developed in section 3. Although it is tempting to choose a very narrow spectrum, it is not typical for natural raindrops.

4.2 Influence of non-homogeneous abscissas

The second test case differs from the reference case insofar as the initial profiles of the abscissas are forced to vary over altitude (the abscissas would otherwise remain constant, see eq. (3.3)).

Hence, within the cloud, a polynomial dependency on the height is assumed for each abscissa. From the abscissas profiles, the corresponding moments are derived, out of which the parameters of a Γ-distribution (eq. (3.1)) can be reconstructed for every point of the space domain. This Γ-distribution acts as initial condition for the spectral model, and the moments are given as input to the QMoM. The process for the design of the initial conditions is explained in further details in

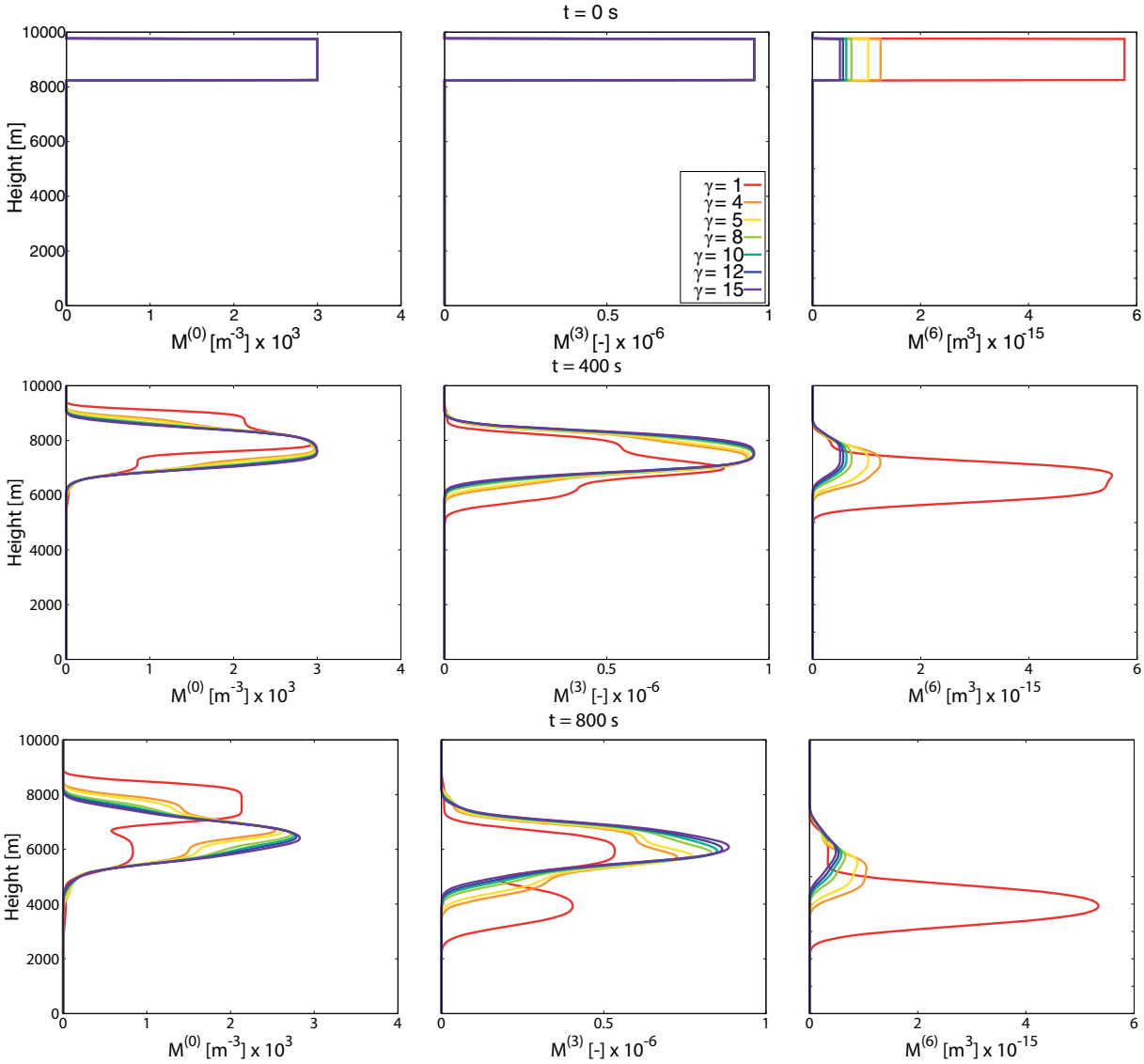

Figure 4: Influence of the initial shape of the PSD: Time evolution of the vertical profile of $M^{(0)}$, $M^{(3)}$, $M^{(6)}$ for QMoM and different Γ-distributions, as in Figure 2, but for $N = 3 \times 10^3\,\mathrm{m}^{-3}$ and $L = 5 \times 10^{-4}\,\mathrm{kgm}^{-3}$. The different shape parameters match those of Fig. 1, left part.

appendix B. As the emphasis is put on the variation of the abscissas over the height, the physical relevance of the moment values has not been meticulously taken into consideration. Nevertheless, the corresponding values of the number density and the liquid water content are of same magnitude as in the previous test cases. This is the reason why only the vertical profile of $M^{(3)}$ is presented here along with the profiles of the abscissas and the weights. The results are shown in Fig. 5 for the QMoM and the DQMoM together with the spectral formulation as reference.

The first important issue raised by the inspection of the abscissas and the weights is the inability of QMoM or DQMoM, in comparison to the spectral model, to depict correctly the evolution of the abscissas near discontinuities (and to some extent those of the weights and the moments). Considering the abscissa e.g., ξ_3 in Fig. 5, we see after 100 s that its profile near the cloud top has not much changed since $t = 0$ s for the QMoM and DQMoM, and we have everywhere a smooth line. For the spectral model, however, ξ_3 has considerably decreased near cloud top and increased near the cloud bottom at around 7000 m. This behavior becomes more pronounced with time as seen after 400 s or 800 s. As such differences near the cloud boundaries between the spectral results and the QMoM results (also for DQMoM) have been also observed for the reference test case (see section 3.2), we deduce that these differences cannot be considered as a consequence of homogeneous abscissas. A possible explanation could be provided by the strong gradients in the profiles of the abscissas and the weights (also the moments), as mentioned by Wright Jr (2007): this hypothesis will be considered and discussed in the next section.

The second main issue deals with the differences between QMoM and DQMoM, although both methods

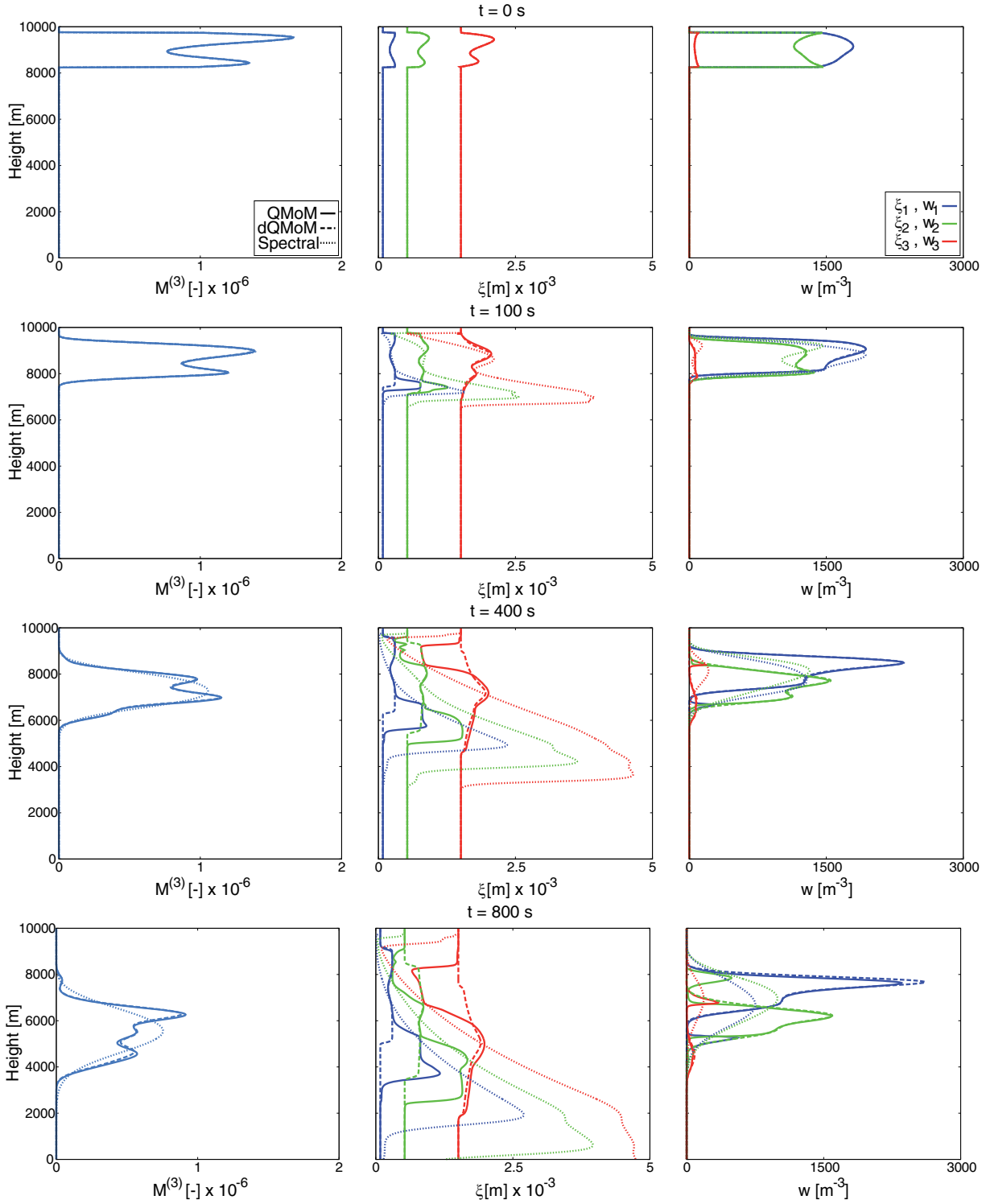

Figure 5: Influence of the initial non-homogeneous abscissas: Time evolution of the vertical profile of $M^{(3)}$, abscissas ξ_i and weights w_i. Solid line: QMoM. Dashed line: DQMoM. Dotted line: spectral method (reference). First, second and third couple of abscissa and weight are plotted in blue, green and red, respectively.

are considered equivalent (see subsections 2.2 and 2.3). Looking at Fig. 5 after 400 s, the profiles of the abscissas ξ_3 close to cloud top differ, and the QMoM-result is closer than the DQMoM-result to the reference solution. The situation is similar close to the cloud base. In order to understand this difference, we have to bear in mind that the DQMoM transports directly the abscissas, while they are reconstructed by the Product-Difference Algorithm (PDA) in the QMoM. This reconstruction process, coupled with numerical differences, allow for deviations, which may amplify with time.

The third issue concerns the QMoM and two abscissas ξ_i and ξ_j which approach each other in the course of time, such as seen in Fig. 5 at $t = 400$ s for (i) ξ_2 and ξ_3 near 8500 m and for (ii) ξ_1 and ξ_2 near 6000 m, and even more distinctly at $t = 800$ s for (i) near 7000 m and for (ii) near 5000 m. When applying the PDA, two abscissas approaching each other means that two eigenvalues of the matrix constructed in the PDA are almost equal (recall that the abscissas are the eigenvalues of this matrix). From a numerical point of view, such a problem is known to be difficult to solve, so that these eigenvalues can be actually found as being equal. In this case, this eigenvalue has two distinct corresponding eigenvectors so that the weights (again, first component of these eigenvectors) cannot be unambiguously affected to one of the two equal abscissas. For instance, if we consider ξ_1 and ξ_2 to become equal, there is no unique way to say which of the two corresponding weights is w_1 or w_2. The possibility for the weights to be interchanged results into the formation of spikes in their profiles, as can be seen in Fig. 5 after 400 s around 8500 m for w_2 and w_3 and even more distinctly after 800 s around 7000 m for w_2 and w_3 and around 5000 m for w_1 and w_2. This coincides with the locations, where corresponding abscissas are almost equal. Notwithstanding, this effect does not affect the profile of the moments, as the latter are obtained through the summation of the weights (with some power of the abscissas as weighting coefficient).

4.3 Influence of sharp gradients in the initial moment profiles

In the third test case, the main idea is to investigate whether spatial discontinuities for the moments at the boundaries of the cloud have an impact on the formation of the modeling artifacts, as seen in section 3.2. We now assume a smooth initial profile for the moments in order to avoid singular behavior with a smooth transition into a cloud free region (see the initial profile of $M^{(3)}$ in Fig. 6). At cloud top, a discontinuity in the moments is kept, however, of smaller amplitude than in the reference case. As for the second test case, the physical relevance of this configuration is insignificant. Further details on the numerical set up are given in appendix C. The evolution of the third moment, the vertical profiles of the abscissas, and the weights are shown in Fig. 6 for both QMoMs with the spectral method as reference. This configuration results in smooth, but height dependent initial profiles of the abscissas.

Figure 6 shows that for the reference solution, sharp gradients develop in the profiles of the abscissas near cloud top. Again, these gradients are better depicted by the QMoM than by the DQMoM, as seen in the precedent section. Nevertheless, both QMoM and DQMoM models are unable to reflect the spatial structure of the profile of the abscissas in the lower part of the model domain. In addition, similarly to the previous test case, we see in the profiles of the weights some spikes pattern, for which the explanation is given in subsection 4.2.

This test case shows that the smooth initial condition with a broader cloud domain than in the previous cases, gives better agreement between the profiles of the moments from the QMoMs and the spectral model. It turns out beneficially that it takes much longer time (compared to test case 2) until the weights separate and segregation effects emerge. Still, the precursor of the segregation is seen in the profile of $M^{(3)}$ after 800 s in the lower model domain.

4.4 Discussions

We have seen the occurrence of the segregation effects in the reference case (Fig. 2) and in the first test case (Fig. 4). They could be interpreted in the case of the homogeneous and thus constant abscissas by the strong dependency of the transport velocities of the weights $V_T(\xi_i)$ on ξ_i, which is a consequence of the diameter dependency of the sedimentation velocity of a drop $V_T(D)$, eq.(2.2). However, these segregation effects are also noticeable in the two other test cases (Figs 5 and 6), showing that a variation of the abscissas does not avoid this problem. Even though the abscissas vary with height, they still are quite distinct, so that the transport velocities for each weight are different and finally lead to the segregation effects. This signifies that, as long as the transport velocities for the abscissas differ from each other, the segregation of the weights cannot be avoided and is therefore inherent to the QMoM and DQMoM. This artifact is independent of a height dependency of the abscissas, yet its outcome is more pronounced for initially homogeneous, hence stationary, ξ_i.

Still the question remains, why QMoM and DQMoM simulations are so strongly affected, while the spectral solution shows nothing of that kind. The QMoM and DQMoM with $N_q = 3$, hence three abscissas and weights, bear resemblance to a spectral model with only three size classes (instead of 500 as in the reference model). If we consider a spectral formulation with very few classes, the transport velocities $V_T(D)$ for each class are different, so that in the pure sedimentation case, such segregation effects between the classes should be expected, resulting in modeling artifacts of the same nature as the step patterns exhibited in the present article. In this case, we expect the characteristic splitting times in the moments to be described as in equation (3.4), but replacing the values of the abscissas by the corresponding diameters of the considered classes. On the other hand, taking more abscissas and weights into account (i.e. $N_q > 3$) and thus more prognostic moments results into more "steps", which however need more time until they can be observed explicitly. Indeed, assuming that a greater N_q implies abscissas closer to each other, so that $(\xi_j^\beta - \xi_i^\beta)$ in eq. (3.4) decreases and the splitting times t_{ij} are therefore longer. This means that in the limit case where a very large number of moments is considered, such that the QMoM methods converge to the spectral one, the splitting times become arbitrarily long.

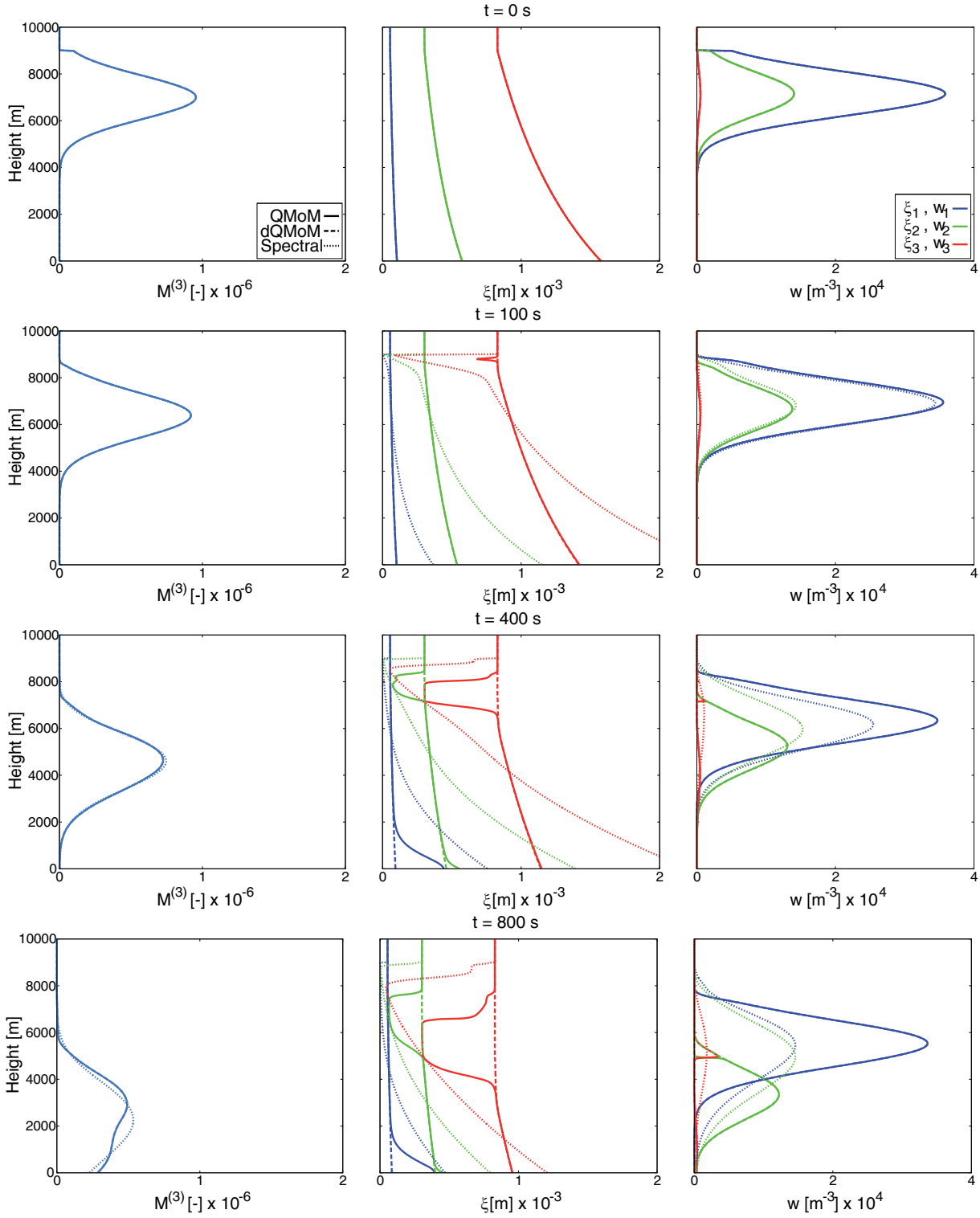

Figure 6: Influence of sharp gradients in the initial vertical distribution of the moments, weights, and abscissas at the cloud limits: Time evolution of the vertical profile of $M^{(3)}$, abscissas ξ_i and weights w_i. Solid line: QMoM. Dashed line: DQMoM. Dotted line: spectral method (reference). First, second and third couple of abscissa and weight are plotted in blue, green and red, respectively.

A common feature to all the test cases presented in this work is that the abscissas ξ_i and weights w_i obtained from the spectral results (reference), therefore considered as the best values, are very different from the abscissas and weights provided by both QMoMs (see notably ξ_i in Figs 2, 3, 5 and 6). The reason for these differences are hypothesized in the case of homogeneous abscissas, but none of the test cases could provide a solid explanation why the differences in a general case are so significant. Further investigation is needed to explain this behavior inherent to the application of QMoMs to the modeling of pure sedimentation of raindrops and, in this way, broaden the knowledge around these QMoM methods.

To sum up, the investigation of the three test cases presented reveals the incapability of both types of QMoM to depict reasonably the profiles of the abscissas and the weights given by the reference solution; therefore they simulate the evolution of the moments only modestly. Moreover, the segregation effects for the weights restrict the reliability of the QMoMs to relatively small sedimentation times. These effects can also lead to unrealizable sets of moments at late sedimentation times, although it is not the case in the results presented in this work. In that case, correction methods for the sets of moments might have to be considered (see for example McGraw (2012)).

However, as demonstrated by Mukhopadhyay et al. (2012) (for which the segregation effects were presumably reduced by a more diffusive numerical scheme for solving the MTE) and by Ziemer et al. (2014) (where QMoM minimizes a quantitative error norm, even if the PMoM considered in this work only consider two prognostic moments as opposed to six for QMoM), both QMoMs remain relevant for modeling the temporal evolution of the moments. The test cases investigated here make explicit the influence of the initial conditions on the modeling artifacts. But they also point out the fact that these methods rely on the evolution of the moments of the PSD and not on the PSD itself, meaning that the actual PSD neither can be reconstructed nor is required.

5 Conclusions

The one dimensional sedimentation reference test case (rainshaft model) presented in this article raises the problem of modeling artifacts inherent to the Quadrature Method of Moment (QMoM). This test case exhibits segregation effects for the weights of the quadrature, which lead to the formation of "step profiles" for the moments. The several other test cases confirm that different initial transport velocities for the weights or the moments lead to the fact that, after some time, the abscissas and weights profiles for the QMoMs do not correspond anymore to the ones obtained from the spectral results. Hence it is concluded that the modeling artifacts are inherent to the method and turn out particularly pronounced during simulation of the sedimentation of drops.

To our knowledge such artifacts have not been reported in other fields of application of the QMoM. We suppose that this could be explained by the diffusive or strong mixing effects induced by the turbulent flow transporting the particles, as commonly seen in engineering applications. Indeed this would result in less differences in the transport velocities for the weights and thus rarer events of separation of regions where the values of the weights are noteworthy. Additionally, the fact that either the particles or the moments are often considered to have the same transport velocity in engineering simulations means that segregation effects may be mostly avoided in these cases. Furthermore, the time scales involved in engineering systems are generally shorter, such that the segregation effects leading to the modeling artifacts exhibited in this work would not have the time to become visible.

Acknowledgments

The authors wish to thank C. Ziemer from Alfred-Wegener-Institut Helmholtz Zentrum für Polar- und Meeresforschung (AWI) and P. Dems from Lehrstuhl für Thermodynamik, Technische Universität München (TUM) for their useful comments and the valuable discussions which have helped to improve the quality of the manuscript. This work was funded by the Deutsche Forschungsgemeinschaft in SPP 1276 MetStröm under grants PO 710/09-[1,2], WA 1334/8-[1,2] and BE 2081/10.

A Transport equations for the weights and abscissas in DQMoM

In their work, Marchisio and Fox (2005) assume a PSD $\hat{f}$ being the weighted sum of Dirac functions (in agreement with the closure approach for the Gaussian Quadrature), that is:

$$\hat{f}(D) = \sum_{i=1}^{N_q} \delta(D-\xi_i) w_i. \tag{A.1}$$

Here, for the same reasons as mentioned for the QMoM (see subsection 2.2), it is assumed $N_q = 3$, but the notation N_q will be kept in the following to save generality. After substitution of $\hat{f}$ into the SBE (2.1) and with the help of derivatives of Dirac functions and the product rule, the SBE is rewritten as:

$$\sum_{i=1}^{N_q} \left[\delta(D-\xi_i) + \delta'(D-\xi_i)\xi_i\right] \underbrace{\left[\frac{\partial w_i}{\partial t} - \frac{\partial V_T(\xi_i) w_i}{\partial z}\right]}_{a_i}$$
$$- \sum_{i=1}^{N_q} \left[\delta'(D-\xi_i)\right] \underbrace{\left[\frac{\partial \zeta_i}{\partial t} - \frac{\partial V_T(\xi_i)\zeta_i}{\partial z}\right]}_{b_i} = 0, \tag{A.2}$$

where ζ_i, $i \in \{1,\ldots,N_q\}$, the so-called weighted abscissas, are defined as:

$$\zeta_i = \xi_i w_i. \tag{A.3}$$

Note that δ' is here an abuse of notation of the derivative of the Dirac function in the mathematical context of distributions. The source terms a_i and b_i for the transport equations for the weighted abscissas $\zeta_i = \xi_i w_i$ and the

weights w_i can be extracted from (A.2) and defined, respectively:

$$\begin{aligned}\frac{\partial w_i}{\partial t} - \frac{\partial V_T(\xi_i) w_i}{\partial z} &= a_i \\ \frac{\partial \zeta_i}{\partial t} - \frac{\partial V_T(\xi_i)\zeta_i}{\partial z} &= b_i,\end{aligned} \tag{A.4}$$

with $V_T(\xi_i)$ given by equation (2.10). Note that the characteristic transport velocities in DQMoM context are therefore transport velocities of abscissas (that is characteristic velocities of drops), while in QMoM context, they are moment velocities, that is integrated means of the velocities of drops (see equation (2.4)). The transport equations for the weighted abscissas and the weights can therefore be seen as a "spectral equivalent" of the MTE for QMoM.

Relying on the properties of the Dirac function:

$$\begin{aligned}\int_0^\infty D^k \delta(D-\xi_i) dD &= {\xi_i}^k \\ \int_0^\infty D^k \delta'(D-\xi_i) dD &= -k{\xi_i}^{k-1},\end{aligned} \tag{A.5}$$

equation (A.2) is moment transformed for each k in $\{0,\ldots,2N_q-1\}$ in order to determine the source terms functions of (A.4). Hence:

$$(1-k)\sum_{i=1}^{N_q} {\xi_i}^k a_i + k\sum_{i=1}^{N_q} {\xi_i}^{k-1} b_i = 0. \tag{A.6}$$

This system can be rewritten in a matrix form $A\sigma = 0$ with $\sigma = \left[a_1,\ldots,a_{N_q},b_1,\ldots,b_{N_q}\right]^T$. As the matrix A is non singular we have $\sigma = 0$ and therefore all source terms of the transport equations for the abscissas and the weights are equal to zero, as shown in (2.9).

We refer to the section 3 of Marchisio and Fox (2005) for further details on the derivation of the equations. Note that in a general formulation, where source terms are considered in the PBE (2.1) (e.g. for coagulation or breakup), source terms also arise in (A.6) (the same ones as those mentioned for the MTE at the end of subsection 2.1) and therefore σ becomes nonzero, meaning a necessary inversion of the matrix A. This matrix inversion can be seen as the counterpart of the PDA in the context of QMoM.

B Initial conditions for test case in subsection 4.2

In this appendix, we derive the values of the vertical profiles for the starting conditions of the test case presented in section 4.2. This is done in three steps.

1. We first consider a configuration analogous to the reference test case (see section 3.1) with the abscissas and weights corresponding to a Γ-distribution (cf. eq. (3.1)) for which $n_0 = 3\times10^3\,\mathrm{m}^{-3}$, $\gamma = 4$ and $\lambda = 1.38\times10^{-4}\,\mathrm{m}$ (that is to say $N = 3\times10^3\,\mathrm{m}^{-3}$ and $L = 4.9538\times10^{-4}\,\mathrm{kgm}^{-3}$ as in Subsection 4.1). The corresponding values for the abscissas and weights (computed with the PDA) are denoted A_i and W_i, respectively: $A_1 = 2.9549\times10^{-4}\,\mathrm{m}$, $A_2 = 7.3354\times10^{-4}\,\mathrm{m}$, $A_3 = 1.450\times10^{-3}\,\mathrm{m}$, $W_1 = 1.4182\times10^3\,\mathrm{m}^{-3}$, $W_2 = 1.4756\times10^3\,\mathrm{m}^{-3}$ and $W_3 = 1.0619\times10^2\,\mathrm{m}^{-3}$. The PSD outside the cloud is assumed to be the same as inside the cloud, but with a scaling factor (10^{-8}) for n_0.

2. In order to dispose of homogeneous profiles for the abscissas, we define three polynomial vertical profiles for the abscissas within the cloud (i.e. for $8250\,\mathrm{m} < z < 9750\,\mathrm{m}$):

$$\hat{\xi}_1(z) = A_1 + \frac{A_1}{2}\left(\frac{z-9000}{750}-1\right)\left(\frac{z-9000}{750}+1\right) \tag{B.1a}$$

$$\hat{\xi}_2(z) = A_2 + A_2\left(\frac{z-9000}{750}-1\right)\left(\frac{z-9000}{750}-\frac{1}{3}\right)\cdot\left(\frac{z-9000}{750}+\frac{1}{3}\right)\left(\frac{z-9000}{750}+1\right) \tag{B.1b}$$

$$\hat{\xi}_3(z) = A_3 - \frac{A_3}{2}\left(\frac{z-9000}{750}-1\right)\left(\frac{z-9000}{750}\right)\cdot\left(\frac{z-9000}{750}+1\right) \tag{B.1c}$$

such that the abscissas are continuous over the height at the cloud boundaries. As for the weights, they are kept unchanged. Following equation (2.7), we obtain the corresponding moments:

$$\hat{M}^{(k)} = \sum_{i=1}^{3} \hat{\xi}_i^k(z) w_i. \tag{B.2}$$

3. As the configuration must be comparable with a spectral method, we reconstruct a Γ-distribution from the three first moments obtained (that is $\hat{M}^{(0)}$, $\hat{M}^{(1)}$ and $\hat{M}^{(2)}$), such that the parameters of this reconstructed PSD (cf eq. (3.1)) are given by:

$$\hat{n_0}(z) = \hat{M}^{(0)} \tag{B.3a}$$

$$\hat{\gamma}(z) = \frac{{\hat{M}^{(1)}}^2}{\hat{M}^{(0)}\hat{M}^{(2)} - {\hat{M}^{(1)}}^2} \tag{B.3b}$$

$$\hat{\lambda}(z) = \frac{\hat{M}^{(0)}\hat{M}^{(2)} - {\hat{M}^{(1)}}^2}{\hat{M}^{(0)}\hat{M}^{(1)}}. \tag{B.3c}$$

This reconstructed PSD is finally given as input to the spectral model, its moments (derived analytically) as input for the QMoM and its abscissas and weights (computed with the PDA) as input to the DQMoM.

Note that, because of the construction and reconstruction processes, the series of moments of the designed Γ-distribution (eq. (B.3)) differs from the moments at the second stage (eq. (B.1)), as only the first three moments are reconstructed exactly. This results in discrepancies in the vertical profiles of the abscissas, which therefore are not equal to the one constructed in the first step, but also in the vertical profiles of the weights which are not homogeneous anymore.

C Initial conditions for test case in subsection 4.3

This appendix gives the numerical values for the vertical profiles for the initial conditions of the test case presented in section 4.3. Once again, we start the design of the set up considering a PSD analogous to the reference test case (see eq. (3.1)), that is a Γ-distribution, for which the parameters are $n_{0r} = 3 \times 10^3\,\mathrm{m}^{-3}$, $\gamma_r = 1$ and $\lambda_r = 3.7575 \times 10^{-4}\,\mathrm{m}$ (that is to say $N_r = 3 \times 10^3\,\mathrm{m}^{-3}$ and $L_r = 5 \times 10^{-4}\,\mathrm{kgm}^{-3}$ as in Subsection 4.1). In order to impose the vertical dependency of the moments (especially the smooth transition from the cloud to the cloud free regions), we scale $M_r^{(0)}$ (which is equal to N_r) and $M_r^{(3)}$ with a Gaussian function over the height. Moreover, to avoid homogeneous abscissas, $M_r^{(0)}$ is scaled with an extra function depending on the height so that:

$$\hat{M}^{(0)}(z) = N_r \left(C_a \frac{z + z_{\mathrm{top}}}{2 z_{\mathrm{top}}} \right)^3 \exp\left(- \frac{(z - z_{\max})^2}{A_a} \right) \tag{C.1a}$$

$$\hat{M}^{(3)}(z) = M_r^{(3)} \exp\left(- \frac{(z - z_{\max})^2}{A_a} \right). \tag{C.1b}$$

z_{top} is the upper limit of the computational domain, that is 10000 m. The parameters $z_{\max}$ and A_a are related to the shape of the Gaussian function: $z_{\max} = 7000\,\mathrm{m}$ is the height where $\hat{M}^{(3)}$ reaches its maximum and $A_a = 10^6 / \ln(10)\ \mathrm{m}^2$ is proportional to the variance of the Gaussian function and thus express the thickness of the cloud. Finally $C_a = 3$ is an amplification factor for the scaling of $\hat{M}^0$.

Considering $\hat{\gamma} = \gamma_r = 1$ everywhere, the parameters of the corresponding Γ-distribution at each height are given by:

$$\hat{n}_0(z) = N_r \left(C_a \frac{z + z_{\mathrm{top}}}{2 z_{\mathrm{top}}} \right)^3 \exp\left(- \frac{(z - z_{\max})^2}{A_a} \right) \tag{C.2a}$$

$$\hat{\lambda}(z) = \left(\frac{2 z_{\mathrm{top}}}{C_a (z + z_{\mathrm{top}})} \right) \sqrt[3]{\frac{M_r^{(3)}}{N_r} \frac{\Gamma(\gamma_r)}{\Gamma(\gamma_r + 3)}}. \tag{C.2b}$$

In a final step, we truncate the vertical profile at the height $z^* = 9000\,\mathrm{m}$ to represent the discontinuity at the upper cloud boundary. For heights above this limit (i.e. for $z^* \le z \le z_{\mathrm{top}}$) we have:

$$\hat{n}_0(z) = 10^{-8} \hat{n}_0(z^*) \tag{C.3a}$$

$$\hat{\lambda}(z) = \hat{\lambda}(z^*). \tag{C.3b}$$

Note that the parameters related to the vertical distribution were chosen arbitrarily to obtain a configuration comparable with the reference study case.

References

Acher, T., P. Dems, S. Lenz, C. Gobert, W. Polifke, 2013: Validation of a quadrature method of moments for polydisperse flow in bubble columns including poly-celerity, breakup and coalescence. – In: 8th Int. Conf. on Multiphase Flows, ICMF 2013, Jeju, Korea.

Beheng, K.D., 1994: A parameterization of warm cloud microphysical conversion processes. – Atmos. Res. **33**, 193–206.

Berry, E.X., R.L. Reinhardt, 1974: An analysis of cloud drop growth by collection: Part II. Single initial distributions. – JAS **31**, 1825–1831.

Clark, T.L., 1974: A study in cloud phase parameterization using the gamma distribution. – J. Atmos. Sci. **31**, 142–155.

Curto, R.E., L.A. Fialkow, 1991: Recursiveness, positivity, and truncated moment problems. – Houston J. Math. **17**, 603–635.

Dems, P., J. Carneiro, W. Polifke, 2012: Large Eddy Simulation of a particle-laden swirling flow with a presumed function method of moments. – Progress Comp. Fluid Dynam. **12**, 92–102.

Gordon, R.G., 1968: Error bounds in equilibrium statistical mechanics. – J. Math. Phys. **9**, 655–663.

Handy, C.R., D. Bessis, T.D. Morley, 1988: Generating quantum energy bounds by the moment method: A linear-programming approach. – Phys. Rev. A **37**, 4557–4569.

John, V., F. Thein, 2012: On the efficiency and robustness of the core routine of the quadrature method of moments (QMOM). – Chem. Engineer. Sci. **75**, 327–333.

Kessler, E., 1969: On the distribution and continuity of water substance in atmospheric circulations. – Amer. Meteor. Soc., Boston, Meteor. Monogr. **32**.

Khain, A., I. Sednev, 1996: Simulation of precipitation formation in the Eastern Mediterranean coastal zone using a spectral microphysics cloud ensemble model. – Atmos. Res. **43**, 77–110.

Marchisio, D.L., R.O. Fox, 2005: Solution of population balance equations using the direct quadrature method of moments. – J. Aerosol Sci. **36**, 43–73.

Marchisio, D.L., R. Vigil, R.O. Fox, 2003: Quadrature method of moments for aggregation-breakage processes. – J. Colloid Interface Sci. **258**, 322–334.

McGraw, R., 1997: Description of aerosol dynamics by the quadrature method of moments. – Aerosol Sci. Technol. **27**, 255–265.

McGraw, R., 2012: Correcting transport errors during advection of aerosol and cloud moment sequences in Eulerian models. – In: Druyan, D.L. (Ed.): Climate Models, InTech, 297–310.

Milbrandt, J.A., M.K. Yau, 2005: A multimoment bulk microphysics parameterization. Part II: A proposed three-moment closure and scheme description. – J. Atmos. Sci. **62**, 3065–3081.

Mukhopadhyay, A., G. Jasor, W. Polifke, 2012: Simulation of pure sedimentation of raindrops using quadrature method of moments. – Atmos. Res. **106**, 61–70.

Patankar, S., 1980: Numerical Heat Transfer and Fluid Flow. – Series in computational methods in mechanics and thermal sciences, Taylor &Francis.

Pitaevskii, L.P., E.M. Lifshitz, 1981: Physical Kinetics. Number 10 in Course of Theoretical Physics by L.D. Landau and E.M. Lifschitz. – Butterworth-Heinemann, Oxford.

Pruppacher, H.R., J.D. Klett, 1997: Microphysics of Clouds and Precipitation. – Kluwer Academic Publishers, Dordrecht, 954 pp.

Ramkrishna, D., 2000: Population Balances: Theory and Applications to Particulate Systems in Engineering. – Academic Press.

Seifert, A., K. Beheng, 2001: A double-moment parameterization for simulating autoconversion, accretion and selfcollection. – Atmos. Res. **59-60**, 265–281.

Seifert, A., K. Beheng, 2006: A two-moment cloud microphysics parameterization for mixed phase clouds. Part 1: Model description. – Meteor. Atmos. Phys. **92**, 45–66.

Seifert, A., C. Köhler, K.D. Beheng, 2012: Aerosol-cloud-precipitation effects over Germany as simulated by a convective-scale numerical weather prediction model. – Atmos. Chem. Phys. **12**, 709–725.

Shohat, J.A., J.D. Tamarkin, 1943: The Problem of Moments. Number 1 in Mathematical Surveys. – American Mathematical Society, Providence, 140 pp.

Wright Jr, D.L., 2007: Numerical advection of moments of the particle size distribution in eulerian models. – J. Aerosol Sci. **38**, 352–369.

Ziemer, C., U. Wacker, 2012: Parameterisation of the sedimentation of raindrops with finite maximum diameter. – Mon. Wea. Rev. **140**, 1589–1602.

Ziemer, C., G. Jasor, U. Wacker, K.D. Beheng, W. Polifke, 2014: Quantitative Comparison of Presumed-Number-Density and Quadrature Moment Methods for Drop Sedimentation. – Meteorol. Z. **23**, 411–423, DOI: 10.1127/0941-2948/2014/0564